Prediction of Secondary Organic Aerosol from the Multiphase Reaction of Gasoline Vapor by Using Volatility–Reactivity Base Lumping

Sanghee Han[1], Myoseon Jang[1]

[1]Department of Environmental Engineering Science, University of Florida, Gainesville, Florida, USA

Correspondence to: Myoseon Jang (mjang@ufl.edu)

Abstract. Heterogeneous chemistry of oxidized carbons in aerosol phase is known to significantly contribute to secondary organic aerosol (SOA) burdens. The UNIfied Partitioning Aerosol phase Reaction (UNIPAR) model was developed to process the multiphase chemistry of various oxygenated organics into SOA mass predictions in the presence of salted aqueous phase. In this study, the UNIPAR model simulated the SOA formation from gasoline fuel, which is a major contributor to the observed concentration of SOA in urban areas. The oxygenated products, predicted by the explicit mechanism, were lumped according to their volatility and reactivity and linked to stoichiometric coefficients which were dynamically constructed by predetermined mathematical equations at different NO_x levels and degrees of gas aging. To improve the model feasibility in regional scales, the UNIPAR model was coupled with the Carbon Bond 6 (CB6r3) mechanism. CB6r3 estimated the hydrocarbon consumption and the concentration of radicals (i.e., RO_2 and HO_2) to process atmospheric aging of gas products. The organic species concentrations, estimated by stoichiometric coefficient array and the consumption of hydrocarbons, were applied to form gasoline SOA *via* multiphase partitioning and aerosol–phase reactions. To improve the gasoline SOA potential in ambient air, model parameters were also corrected for gas–wall partitioning (GWP). The simulated gasoline SOA mass was evaluated against observed data obtained in the UF-APHOR chamber under varying sunlight, NO_x levels, aerosol acidity, humidity, temperature, and concentrations of aqueous salts and gasoline vapor. Overall, gasoline SOA was dominantly produced via aerosol–phase reaction, regardless of the seed conditions owing to heterogeneous reactions of reactive multifunctional organic products. Both the measured and simulated gasoline SOA was sensitive to seed conditions showing a significant increase in SOA mass with increasing aerosol acidity and water content. A considerable difference in SOA mass appeared between two inorganic aerosol states (dry aerosol vs. wet aerosol) suggesting a large difference in SOA formation potential between arid (Western United States) and humid regions (Eastern United States). Additionally, aqueous reactions of organic products increased the sensitivity of gasoline SOA formation to NO_x levels as well as temperature. The impact of the chamber wall on SOA formation was generally significant, and it appeared to be higher in the absence of wet salts. Based on the evaluation of UNIPAR against chamber data from 10 aromatic hydrocarbons and gasoline fuel, we conclude that the UNIPAR model with both heterogeneous reactions and the model parameters corrected for GWP can improve the ability to accurately estimate SOA mass in regional scales.

1 Introduction

The atmospheric oxidation of hydrocarbons (HCs) produces ozone in the troposphere through a photochemical cycle of nitrogen oxides. This ozone can increase the risks of respiratory disease (Jerrett et al., 2009), cardiovascular disease, and premature death (Turner et al., 2016). Additionally, the atmospheric process of HCs can produce semivolatile oxygenated products that can form secondary organic aerosol (SOA) through either gas–particle partitioning or aerosol–phase reactions. SOA is a major contributor to the fine particular matter ($PM_{2.5}$) in ambient air (Jimenez et al., 2009), with significant effects on climate (Heald et al., 2008) and human health (Cohen et al., 2017;Pöschl, 2005). Thus, it is critical to understand and

predict the amount of SOA produced from the atmospheric oxidation of various HCs to effectively improve air quality and human health.

40   The air quality models, integrated with the partitioning based SOA module using two (Odum et al., 1996) or several surrogate species (i.e., Volatility Basis Set (Donahue et al., 2006)), tend to underpredict SOA mass in the urban ambient air (Volkamer et al., 2006;Dzepina et al., 2011;Ensberg et al., 2014;Hayes et al., 2015;Appel et al., 2017;Woody et al., 2016). Much effort has been given to reduce the model–measurement discrepancies by adding missing SOA precursors (McDonald et al., 2018), including heterogeneous reactions (Carlton et al., 2010), and correcting the SOA model parameters by

45   considering gas–wall partitioning (GWP) bias (Cappa et al., 2016;Baker et al., 2015;Hayes et al., 2015). For example, high SOA yields (>0.1) were reported from several individual intermediate volatility compounds in consumer product mixtures (Li et al., 2018). Thus, the extension of the SOA model to additional precursors emitted from the commercial usage of chemicals was attempted to close the model-measurement gap (Qin et al., 2021;Shah et al., 2019;McDonald et al., 2018).

The oligomers in SOA formed from photooxidation of precursor HCs in chambers and the ambient air has been identified as

50   25-70% of the SOA mass (Kalberer et al., 2004;Tolocka et al., 2004;Gross et al., 2006;Kalberer et al., 2006;Hallquist et al., 2009). Thus, there have been numerous implications of in-particle chemistry in SOA formation for the model studies (Carlton and Turpin, 2013;Carlton et al., 2010;Pye et al., 2017). For example, the formation of oligomers was considered in the SOA module of Community Multiscale Air Quality (CMAQ) as a first order reaction of condensed organic species, resulting in the improvement of spatial and temporal trends of SOA mass in particular for biogenic SOA (Carlton et al.,

55   2010). To introduce the role of aerosol water contents in SOA formation, Jathar et al. (2016) examined the water uptake to the organic phase in SOA model and assess its influence on SOA formation (Jathar et al., 2016). Moreover, Pye et al. (2017) evaluate the importance of aerosol-water-organic interactions in the CMAQ model accounting for the uptake of water onto the hydrophilic organics (Pye et al., 2017). Despite such efforts, the performance of SOA formation in representing spatial and seasonal variation in ambient aerosol tends to underestimate total aerosol mass in the southern and western US (Appel et

60   al., 2021).

Inaccuracy of SOA predictions can be originated from the integration of the SOA model with the model parameters originated from biased chamber data. The deposition of organic vapor onto the reactor wall can cause the negative bias in SOA prediction because SOA model parameters are typically determined on the basis of a mass balance by using chamber data (Matsunaga and Ziemann, 2010;Zhang et al., 2014;Yeh and Ziemann, 2015;Krechmer et al., 2016;Huang et al., 2018).

65   Thus, the GWP of semivolatile organic compounds was semiempirically characterized for various organic species. Many model studies reported that the significance of GWP varied with precursor HCs, gas oxidation process (different NO_x levels or oxidants), chamber dimension and size, seed conditions, and meteorological conditions (temperature and humidity) (Zhang et al., 2014;Krechmer et al., 2020;Brune, 2019;Huang et al., 2018;Cappa et al., 2016). To simulate SOA formation accurately, the integration of the GWP model to the SOA model is inevitable in chamber studies. However, the application

70   of individually determined GWP bias in the air quality model is challenging due to the surrogate species in air quality models.

In this study, the SOA formation from photooxidation of gasoline vapor was simulated with the UNIfied Partitioning Aerosol-phase Reaction (UNIPAR) model, which predicts SOA formation via multiphase reactions. The important feature of the UNIPAR model is to simulate SOA formation via aqueous phase reactions of organic species in the absence of GWP.

75   The UNIPAR model streamlines gas oxidation mechanisms, multiphase partitioning (gas, organic phase, and inorganic salted solution), and aerosol-phase reactions in both organic and inorganic phases (Beardsley and Jang, 2016;Im et al., 2014;Zhou et al., 2019;Yu et al., 2021). The model parameters and equations in the model have been demonstrated for various SOA produced from aromatic HCs (Im et al., 2014;Zhou et al., 2019), terpenes (Yu et al., 2021), and isoprene

(Beardsley and Jang, 2016). In order to predict SOA mass in ambient air, the model parameters were updated by using the GWP model that employed a quantitative structure activity relationship (QSAR) approach (Han and Jang, 2020). The Carbon Bond 6 (CB6r3) (Yarwood et al., 2010) mechanism was integrated with UNIPAR to obtain the consumption of HCs and the concentration of radicals (RO_2 and HO_2) that processed atmospheric aging. The simulated SOA mass was compared to chamber generated SOA data under the University of Florida Atmospheric PHotochemical Outdoor Reactor (UF-APHOR). The UNIPAR prediction was also compared to the prediction from the AERO7 module in CMAQ model (CMAQ-AE7) (Appel et al., 2021). The sensitivity of gasoline SOA formation to various environmental conditions, such as temperature, relative humidity (RH), seed conditions, and the concentration of HC, was investigated.

2 Chamber experiment

Gasoline SOA was generated from the photooxidation of US commercial gasoline vapor (octane numbers of 87) under ambient sunlight in the UF-APHOR outdoor chamber located on the rooftop of Black Hall (29.64˚, -82.34˚) at the University of Florida, Gainesville, Florida. Based on the gas chromatography–flame ionization detector (GC–FID, HP-5890/Agilent Technologies 7820A) analysis of injected gasoline vapor, 30% of carbons in the gasoline were from single-ring aromatic HCs (Fig. S1). The gasoline vapor, NO_x, and inorganic seed aerosols were injected into the chamber before sunrise, and experiments were conducted for 10 hours after sunrise. The NO_x level was classified into high NO_x ($HC/NO_x < 5.5$ ppbC/ppb) and low NO_x level ($HC/NO_x > 5.5$ ppbC/ppb) based on the initial concentration of HC and NO_x. Four different seed conditions (non-seeded (NS); sulfuric acid (SA); wet ammonium sulfate (wAS); dry ammonium sulfate (dAS)) were applied to evaluate the seed effects on gasoline SOA. The chamber conditions for conducted experiments were summarized in Table 1.

The concentration of HCs and CCl_4 were monitored using a GC–FID. The measured HC concentration from GC–FID determined HC consumption in the chamber during the experiment. The concentration of CCl_4 was measured as a function of time to obtain the dilution factor in the chamber. The concentrations of O_3 and NO_x were monitored with a photometric ozone analyzer (Teledyne, model 400E) and a chemiluminescence NO/NO_2 analyzer (Teledyne, model 200E), respectively. The measurement of inorganic ion (SO_4^{2-} and NH_4^+) and organic carbon (OC) concentrations of aerosol were conducted with in situ monitoring by the Particle-Into-Liquid-Sampler (Applikon, ADI 2081) coupled with Ion Chromatography (Metrohm, 761Compact IC) (PILS–IC) and an OC/EC carbon aerosol analyzer (Sunset Laboratory, Model 4), respectively. The particle volume concentration was monitored with a Scanning Mobility Particle Sizer (SMPS, TSI, Model 3080) integrated with a condensation nuclei counter (TSI, Model 3025A and Model 3022). The composition (SO_4^{2-}, NO_3^-, NH_4^+, and organic) of aerosol was also monitored using an Aerosol Chemical Speciation Monitor (ACSM, Aerodyne Research Inc., USA) to compare with the data obtained from OC and PILS–IC for the accurate measurement. The meteorological factors (RH, temperature, and ultraviolet radiation) were measured in the UF-APHOR and applied to the simulation. The sunlight intensity is measured by Total Ultraviolet Radiometer (EPLAB, TUVR). Aerosol acidity (mol/L of aerosol) was monitored by colorimetry integrated in the reflectance UV–visible spectrometer (Li and Jang, 2012;Jang et al., 2020).

3 Model descriptions

The UNIPAR model was coupled with CB6r3 gas mechanism to simulate SOA formation from photooxidation of HCs (UNIPAR-CB6r3). The overall structure of the UNIPAR-CB6r3 model is illustrated in Fig. 1. The main feature of the model is the SOA simulation based on volatility and reactivity of organic products by using lumping species that are constructed from explicit gas products. In UNIPAR-CB6r3, the model parameters are corrected by the GWP artifacts, and they are also universalized for 10 aromatic HCs to predict SOA formation from gasoline vapor. The UNIPAR-CB6r3 model was

simulated in the Dynamically Simple Model of Atmospheric Chemical Complexity (DSMACC) (Emmerson and Evans, 2009) integrated with the Kinetic PreProcessor (KPP) (Damian et al., 2002).

120 The CB6r3 mechanism simulates the atmospheric oxidation of anthropogenic precursors in the gas phase and yields the consumption of HCs (ΔHC) and concentration of RO$_2$ ([RO$_2$]) and HO$_2$ ([HO$_2$]). In the model, the predetermined polynomial equations, derived by using explicit gas mechanisms (Master Chemical Mechanism, MCM v3.3.1) (Jenkin et al., 2012), estimate the stoichiometric coefficients (α_i) of the lumping species (i) of gas phase oxygenated products. The quantity of α_i array, which classified into 51 lumping species according to their volatility and reactivity in the aerosol–phase, are dynamic

125 as a function of a HC/NO$_x$ level and degree of aging, which is calculated with ΔHC, [RO$_2$], and [HO$_2$] from CB6r3. These lumping species are then used to generate SOA mass (OM$_T$) via gas–particle partitioning (OM$_P$) and heterogeneous reactions (OM$_{AR}$) in both organic and inorganic phases. The SOA formation via aqueous phase reactions of organic species was simulated under the assumption of the liquid-liquid phase separation (LLPS) between organic and inorganic phase. The details of the model description are shown in the following sections.

130 **3.1 Lumped Organic Species**

The formation of oxygenated products is predicted by simulating the MCM v3.3.1 gas mechanism. The resulting oxygenated products are, then, classified into 51 lumping species based on their volatility and chemical reactivity. α_i is determined at varying HC/NO$_x$ ratios and the different degree of gas aging, and dynamically constructed by using the mathematical equations based on the simulation of MCM v.3.3.1. The degree of aging is mathematically correlated with the concentration

135 of RO$_2$ and HO$_2$, which are normalized with the initial concentration of HCs. These lumping species are linked to a mass-based α_i to produce the concentrations of each lumping species. In order to process the multiphase thermodynamic equilibrium of lumping species (i), the physicochemical properties (vapor pressure ($p_{L,i}^\circ$), molecular weight (MW_i), oxygen to carbon ratio ($O{:}C_i$), and hydrogen bonding (HB_i)) are determined based on the group contribution (Stein and Brown, 1994). In the UNIPAR model, the volatilities of each oxidation product are classified into eight levels of the vapor pressure

140 ($P_{L,i}^\circ$) (1–8: 10^{-8}, 10^{-6}, 10^{-5}, 10^{-4}, 10^{-3}, 10^{-2}, 10^{-1}, and 1 mmHg) and six levels based on the aerosol–phase reactivity scale (R_i): very fast (VF), fast (F), medium (M), slow (S), partitioning only (P), and multi-alcohol (MA) and three additional reactive species (glyoxal, methylglyoxal, and epoxydiols).

In UNIPAR-CB6r3, the UNIPAR model is coupled with the CB6r3 mechanism (Yarwood et al., 2010) that is used in air quality models. The CB6r3 mechanism has been frequently used to predict the ozone formation by using a unique lumping

145 species (Yarwood et al., 2005;Yarwood et al., 2010) but is limited to consider the physicochemical properties of oxygenated products, which are necessary to process SOA formation. In CB6r3, the reaction of toluene or benzene with an OH radical is explicitly expressed. In order to obtain ΔHC from each aromatic HC, the reactions of other aromatic HCs (i.e., ethylbenzene, propylbenzene, 3 xylene isomers, and 3 trimethylbenzene isomers) with an OH radical were explicitly treated by using individual reaction rate constants (Table S1). In this study, ΔHC, [RO$_2$], and [HO$_2$] are obtained from CB6r3 and

150 incorporated with predetermined polynomial equations to determine the α_i array as a function of HC/NO$_x$ ratios and an aging scale (Fig. 1). These equations are mathematically derived by using explicit products predicted from MCM v3.3.1. The gas concentration ($C_{g,i}$) of lumping species, i, is estimated by multiplying ΔHC by dynamically predicted α_i (Zhou et al., 2019). The physicochemical parameter arrays (MW_i, $O{:}C_i$, and HB_i) are unified by using 51 lumping species for 10 different aromatic HCs and they are applied to estimate multiphase partitioning and aerosol's medium properties.

155 **3.2 Multiphase Partitioning**

The gas products produced from the atmospheric oxidation of precursor HCs partition onto both organic and inorganic phase ($C_{or,i}$ and $C_{in,i}$, respectively). $C_{or,i}$ and $C_{in,i}$ are incorporated into in-particle chemistry to form OM$_{AR}$ (Fig. 1). In this model,

the gas–particle partitioning processes are assumed as an equilibrium partitioning process based on the absorptive partitioning theory (Pankow, 1994), which assumes that the gas–particle partitioning instantaneously reaches equilibrium to distribute the gas products into the gas, organic and inorganic phases.

The partitioning coefficient of i into the organic phase ($K_{or,i}$) and inorganic phase ($K_{in,i}$) are determined by the traditional absorptive partitioning theory (Pankow, 1994) as follows:

$$K_{or,i} = \frac{7.501RT}{10^9 MW_{or}\gamma_{or,i}p^{\circ}_{L,i}}, \tag{1}$$

$$K_{in,i} = \frac{7.501RT}{10^9 MW_{in}\gamma_{in,i}p^{\circ}_{L,i}}, \tag{2}$$

where MW_{or} (g mol^{-1}) is the molecular weight of OM$_T$, R (8.314 J mol^{-1} K^{-1}) is the ideal gas constant, and T (K) is the temperature. $\gamma_{or,i}$ is the activity coefficient of i in organic phase. MW_{in} is the averaged molecular weight of inorganic aerosol, and $\gamma_{in,i}$ is the activity coefficient of i in inorganic phase. $\gamma_{or,i}$ is assumed as unity, while $\gamma_{in,i}$ is semiempirically estimated with a polynomial equation, determined by fitting the $\gamma_{in,i}$ estimated by the Aerosol Inorganic–Organic Mixtures Functional groups Activity Coefficient (AIOMFAC) (Zuend et al., 2011):

$$\gamma_{in,i} = e^{0.035MW_i - 2.704\ln(O:C_i) - 1.121HB_i - 0.33FS - 0.022(RH)}, \tag{3}$$

where RH is relative humidity (%), and FS (fractional sulfate, FS = [SO$_4^{2-}$]/([SO$_4^{2-}$]+[NH$_4^+$])) is the concentration ratio of total sulfate to the sum of total sulfate and ammonium ions in aerosol (Zhou et al., 2019). In the model, FS, introduced to determine aerosol acidity, ranges from 0.334 for AS to 1 for SA. To simulate the gasoline SOA, unified matrix of MW_i, $O:C_i$, and HB_i for 51 lumping species were applied to the SOA prediction from 10 different aromatic HCs, which are the compositions of gasoline vapor.

3.3 OM$_{AR}$: SOA growth via aerosol–phase reactions

OM$_{AR}$ is produced via oligomerization in both organic and inorganic phases, as described in previous studies (Im et al., 2014;Zhou et al., 2019). OM$_{AR}$ is estimated as a second order reaction product from condensed organics based on the assumption of a self-dimerization reaction of organic compounds in media (Odian, 2004):

$$\frac{dC'_{or,i}}{dt} = -k_{o,i}C'^2_{or,i}, \tag{4}$$

$$\frac{dC'_{in,i}}{dt} = -k_{AC,i}C'^2_{in,i}, \tag{5}$$

where $C'_{or,i}$ and $C'_{in,i}$ are the concentration of i in the organic and inorganic aerosol phase (mol L^{-1}), respectively. The reaction rate constant in the aqueous phase ($k_{AC,i}$) and organic phase ($k_{o,i}$) are determined:

$$k_{AC,i} = 10^{0.25pK_{BH_i^+}+1.0X+0.95R_i+\log(a_w[H^+])-2.58}, \tag{6}$$

$$k_{o,i} = 10^{0.25pK_{BH_i^+}+0.95R_i+5.2\left(1-\frac{1}{1+e^{0.2(270-MW_{or})}}\right)+\frac{2.7}{1+e^{11(0.85-O:C)}}-10.07}, \tag{7}$$

where $k_{AC,i}$ is semiempirically defined as a function of R_i, the protonation equilibrium constant ($pK_{BH_i^+}$), excess acidity (X) (Cox and Yates, 1979;Jang et al., 2006), water activity (a_w), and the proton concentration [H$^+$] (Im et al., 2014;Zhou et al., 2019). $k_{o,i}$ is determined without X, a_w, and [H$^+$] terms because a_w, [H$^+$], and X converged to zero in the absence of wet inorganic seed. In our previous work (Jang et al., 2005;Jang et al., 2006), a 2nd order $k_{AC,i}$ (L mol^{-1} s^{-1}) was described via a rate determining step for polymerization to form polyacetal. $k_{o,i}$ is determined by extrapolating $k_{AC,i}$ to the neutral condition in the absence of salted aqueous solution to process oligomerization in organic phase.

SOA formation in the aqueous phase may not be affected by viscosity because of abundant water molecules, while SOA formation in organic phase can be impacted by viscosity. In the traditional SOA models, it often assumes that the equilibrium in gas–particle partitioning is rapidly achieved. However, studies have shown the relatively long characteristic

time of less volatile organic species onto the semisolid particle to reach equilibrium (Shiraiwa and Seinfeld, 2012;Shiraiwa et al., 2011). In general, the higher viscosity appears with an organic compound with the higher MW (Koop et al., 2011). Although the high O:C ratio (higher polarity) can increase viscosity, polar aerosol can absorb water in some degree at high humidity increasing fluidity. Studies showed that viscosity can also influence chemical reaction rate, limited by slow bulk diffusion within a particle (De Schrijver and Smets, 1966;Reid et al., 2018). In the current knowledge, it is difficult to distinguish the impact of viscosity on the partitioning process from that on reaction rates. In this study, the impact of aerosol viscosity on SOA formation was related to heterogeneous reactions in the organic phase by controlling their reaction rate constant. The sigmoidal functions for MW_{or} and $O:C$ are involved in $k_{o,i}$ to consider the viscosity of organic aerosol.

3.4 OM$_P$: SOA formation via partitioning

It is assumed that gas–organic partitioning is governed by Raoult's law in that the saturation vapor pressure of the species is dependent on the mole fraction of the species in the solution. To consider the subtracted mass in total concentration ($C_{T,i} = C_{g,i} + C_{or,i} + C_{in,i}$) of i by oligomerization, OM$_P$ is recalculated after OM$_{AR}$ integration with the partitioning model (Schell et al., 2001) which is reconstructed by including OM$_{AR}$ (Cao and Jang, 2010). OM$_P$ is estimated from $C_{T,i}$ using a mass balance equation and solved by the Newton Raphson method (Press et al., 1992):

$$OM_P = \sum_i [C_{T,i} - OM_{AR,i} - C_{g,i}^* \frac{\left(\frac{C_{or,i}}{MW_i}\right)}{\sum_i \left(\frac{C_{or,i}}{MW_i} + \frac{OM_{AR,i}}{MW_{oli,i}}\right) + OM_0}], \tag{8}$$

where $C_{g,i}^* (= \frac{1}{K_{or,i}})$ is the effective saturation concentration of i, OM_0 (mol m^{-3}) is the pre-existing OM concentration, and $MW_{oli,i}$ (g mol^{-1}) is the molecular weight of the dimer.

3.5 Model parameters in the absence of GWP bias

The model parameters inherited from chamber-generated SOA mass can be biased and increase inaccuracy in prediction of SOA mass in ambient air. In this study, the UNIPAR-CB6r3 simulation was performed with the model parameters that were not biased by GWP. Regardless of the absence or the presence of GWP, the prediction of OM$_P$ is approached by a fundamental partitioning theory. The modification was mainly made for the model parameters associated with aerosol–phase reaction rate constants of lumping species (i.e., $k_{o,i}$). Consequently, the change in OM$_{AR}$, predicted with the new model parameters, modulates OM$_P$ (Fig. 1).

In order to establish $k_{o,i}$ in the absence of GWP on the model, UNIPAR was integrated with explicit gas mechanisms (MCM v3.3.1) and the GWP model (UNIPAR-GWP, in Sect. S2) (Han and Jang, 2020). Multiphase HC reactions, including gas phase oxidation, gas–particle partitioning, aerosol–phase reactions in organic phase and inorganic aqueous phase, and GWP, were kinetically treated in the model (Fig. S2) by using the absorption rate constants (kon_w) and desorption rate constants ($koff_w$) of organic species i, in wall (w) phases. In UNIPAR-GWP, the GWP processes were predicted with GWP model parameters (organic vapor-wall partitioning and its accommodation coefficient) and the chamber specific characteristics (chamber dimension and the organic matter concentration on the wall). The QSAR approach that employed organic physicochemical parameters facilitated the derivation of the semiempirical polynomial model to predict GWP model parameters, as described in the previous study (Han and Jang, 2020). The $k_{o,i}$ values were amended to predict aromatic SOA by using UNIPAR-GWP against chamber-generated data. The amended $k_{o,i}$ was then applied to the UNIPAR-CB6r3 model to predict the gasoline SOA formation potential in this study.

4 Results and Discussions

4.1 Aromatic SOA simulation with UNIPAR-CB6r3

The gasoline fuel is the mixture of various HCs including aromatics, alkenes, alkanes, and ethanol. It has been known that the photooxidation of aromatic HCs in the presence of NO_x mainly attributes to gasoline SOA (Gentner et al., 2017). Thus, the feasibility of UNIPAR-CB6r3 was evaluated for the prediction of the SOA formation from photooxidation of aromatic HCs in gasoline against chamber-generated SOA data (Table S2). In Fig. 2, the simulation was plotted against chamber-generated SOA mass produced from the photooxidation of 10 different aromatic HCs under various experimental conditions (Table S2). Overall, the predicted SOA mass with UNIPAR-CB6r3 in the presence of GWP agreed well with the observed SOA mass (slope = 1.04 and R^2 = 0.89). Figure S3 illustrates the simulated (solid line) and observed (symbol) concentration of NO, NO_2, O_3 and HC over the course of the experiment. Figure S4 shows a time profile of simulated OM_T (solid line), simulated OM_P (dotted line) and observed SOA data (symbol) over the course of the chamber experiment. A significant contribution of OM_{AR} to OM_T suggests an importance of heterogeneous reactions in SOA formation. The oligomers in SOA formed from photooxidation of precursor HCs in chambers and the ambient air has been identified as a considerable fraction in the SOA mass (Kalberer et al., 2004;Tolocka et al., 2004;Gross et al., 2006;Kalberer et al., 2006;Hallquist et al., 2009).

To characterize the impact of GWP on aromatic SOA formation, the aromatic SOA mass (C_{SOA}, μg m^{-3}) in the absence of GWP bias was plotted versus the aromatic SOA mass ($C_{SOA,wall}$, μg m^{-3}) predicted in the presence of the GWP (Fig. 3). The SOA formation was simulated at (a) high NO_x level (HC/NO_x= 3 ppbC/ppb) and (b) low NO_x level (HC/NO_x= 10 ppbC/ppb) at the given reference conditions (298K, 60% RH) under the specific sunlight intensity measured on 06/19/2015 (Fig. S5(a)). In Fig. 3, the more deviated plot from the 1:1 line indicates the larger impact of GWP on SOA formation. Impact of GWP on SOA formation differs with oxidation product distributions according to volatility and reactivity. The estimated $kon_{w,i}$ of i to the chamber wall was ~5×10^{-4} s^{-1} for UF-APHOR chamber. Similar to OM_P, the impact of GWP on SOA formation is significant in the HCs with low volatile products. The HC with the higher impact of OM_{AR} on OM_T is less influenced by GWP. The characteristic time of aerosol–phase reactions that lead OM_{AR} is generally shorter than that of GWP (Han and Jang, 2020). In the UNIPAR model, the formation of OM_{AR} is irreversible to form nonvolatile oligomer products. Benzene SOA, which is mainly attributed to OM_{AR}, was little influenced by GWP. The oxygenated products from benzene are highly reactive in aerosol phase leading a high contribution of OM_{AR} to OM_T, but they are volatile lowering OM_P as well as the impact of GWP. In case of high NO_x level, SOA mass from the photooxidation of benzene increased as a factor of 1.04 after GWP correction, which is insignificant compared to other aromatic HCs which can produce 1.14-4.75 times higher SOA mass in the absence of GWP impact. The impact of GWP on SOA formation in the presence of inorganic seed (wAHS in red and wAS in blue) was significantly less than that without the wet inorganic seed (black). In the presence of wet seed, plots are much less deviated from the one-to-one line as seen in Fig. 3 in comparison to no-seeded SOA. The C_{SOA} to $C_{SOA,wall}$ ratio are higher under the NS condition (~4.75) than that in the presence of wAHS (~2.54). This tendency agreed with the previously reported results (Krechmer et al., 2020;Zhang et al., 2014). The SOA formation pathway via aqueous reactions of organic products show little sensitivity to GWP.

4.2 Gasoline SOA simulation with UNIPAR-CB6r3

Figure 4 shows the time profiles of simulated OM_T (solid line), OM_{AR} (dotted line), and observed organic matter (symbols) under the experimental conditions summarized in Table 1. Overall, the gasoline SOA mass predicted by UNIPAR-CB6r3 in the presence of wall agrees with SOA mass generated in UF-APHOR under varying NO_x levels and seed conditions. Similar to aromatic SOA (Fig. S4), gasoline SOA formation was dominated by OM_{AR}. SOA mass at the low NO_x level is higher than that at the high NO_x level (Fig. 4(a) vs. 4(b)), causing higher contribution of OM_P to the higher OM_T. At the high NO_x level,

organonitrates and peroxyacetyl nitrate are produced via the reaction of a peroxy radical (RO$_2$) with NO$_2$. Additionally, at the high NO$_x$ level, atmospheric processes yield fewer highly volatile chemical species (i.e., carbonyls, hydroxy carbonyls) (Hallquist et al., 2009) because OH radicals tend to react with NO$_2$ to form HNO$_3$.

A significant enhancement of gasoline SOA mass was observed in the presence of acidic seed (Fig. 4(b) vs. 4(c)) or wet seed (Fig. 4(e)). The electrolytic inorganic particle can contain a significant amount of aerosol water above efflorescence RH (ERH) or deliquescence RH (DRH). When the inorganic aerosol is wet, reactive organic species can heterogeneously react in aqueous phase and increase SOA mass. The UNIPAR-CB6r3 model simulation shows the importance of aqueous reactions of reactive organic products to increase SOA mass. In the current model, produced gasoline SOA mass is not subtracted from the gas phase. Thus, the model can cause inaccuracy particularly for a high yield SOA system. For example, the gasoline SOA yield in the presence of acidic seed under the low NO$_x$ level is high, and this presumably would cause the overestimation of SOA mass as seen in Fig. 4(d).

The gasoline SOA was produced in the presence of different amounts of wAS (excluding water mass) as 50 µg m^{-3} (Fig. 4(e)) and 120 µg m^{-3} (Fig. 4(f)). However, the influence of the concentration of wAS is trivial in both simulation and observations. This tendency indicates that a certain quantity of wAS is enough to rapidly progress aqueous reactions of reactive organic species. Figure 4(g) demonstrates the impact of the aerosol phase on SOA formation, showing a significantly different SOA growth rate after 1 PM where RH dropped lower than ERH (changing from wAS to dAS).

Figure 5 shows the impact of GWP on chamber-generated SOA (Table 1). Similar to aromatic SOA, the impact of GWP on SOA is greater with the higher NO$_x$ level because peroxyacyl nitrates and organonitrates, which are little reactive in aerosol phase, can attribute to SOA mass (Fig. 5(a)vs. Fig. 5(b)). In the presence of acidic seed (Fig. 5(c)) or wAS (Fig. 5(d)), gasoline SOA formation is less affected by GWP.

The UNIPAR-CB6r3 model simulation (Fig. 4(a) and 4(b)) in the presence of GWP was compared to that predicted with CMAQ-AE7 as seen in Fig. S6. For SOA formation via gas–particle partitioning of semivolatile compounds in CMAQ-AE7, 4 surrogate compounds produced from anthropogenic precursors (i.e., aromatic HCs, long chain alkanes, and polycyclic aromatic hydrocarbons) are employed (Qin et al., 2021). The non-volatile species that are predominantly present in particle phase are also included. The first order oligomerization reaction of organic species is included in gas mechanisms. A distinguishable difference between two models is oligomeric fraction in SOA mass. A small fraction of SOA mass predicted with CMAQ-AE7 (Fig. S6) is attributed to oligomeric matter (~10%), while SOA mass predicted with UNIPAR-CB6r3 (Fig. 4) is dominantly attributed to OM$_{AR}$ (~80%). Laboratory studies report that 25% to 80% of SOA mass are oligomeric matter (Hallquist et al., 2009;Hall IV and Johnston, 2011;Kalberer et al., 2006). For the ozonolysis of α-pinene, Hall and Johnston reported that the weight percentage of oligomers was estimated to be more than 50% (Hall IV and Johnston, 2011). The oligomeric fraction in 1,3,5-trimethylbenzene SOA was reported as 50-60% after 5-6 hr and increased up to 80% after 25 hr (Kalberer et al., 2006).

4.3 Sensitivity and Uncertainties

Figure 6 simulates the sensitivity of gasoline SOA to environmental variables (temperature, initial gasoline vapor concentration, RH, aerosol acidity, and seed concentration). The SOA mass that predicted different environmental conditions were compared to that of the predicted at the given reference condition (60% RH, 298 K, and HC/NO$_x$=3 ppbC/ppb) under the sunlight intensity measured on 6/19/2015 (Fig. S5(a)). The wet inorganic seed concentration was 10 µg m^{-3}, and the preexisting organic matter concentration was 3 µg m^{-3}. The initial gasoline vapor concentration was 1500 ppbC. In addition to the UNIPAR-CB6r3 simulation, the SOA formation was also predicted by the aerosol module in CMAQ-AE7.

In Fig. 6(a), the sensitivity of SOA formation to temperature was simulated between 278K and 318K. Gas–particle partitioning of reactive organic products increases with decreasing temperature, and consequently SOA formation via aqueous reaction increases. There, the high sensitivity of SOA growth to temperature appears with wet seed aerosol compared to no seeded SOA. The SOA simulation with the CMAQ-AE7 module shows a little sensitivity to temperature compared to the UNIPAR-CB6r3 simulation. Gasoline SOA formation was simulated with various initial concentrations of gasoline vapor ranging from 50 ppbC to 1500 ppbC. The SOA mass was plotted to the consumption of aromatic HCs at a given initial gasoline vapor concentration in Fig. 6(b). The consumption of aromatic HC is not linearly related to the initial gasoline vapor concentration. The SOA mass shows a curved shape indicating the partitioning contribution on the SOA growth. At the maximum SOA yield, the constant slope appears. Figure 6(c) illustrates the impact of NO_x levels on gasoline SOA formation. All three simulated SOA mass are negatively correlated to NO_x levels as seen in several studies (Zhou et al., 2019;Im et al., 2014). The SOA formation in the presence of aqueous salted solution gradually increases with higher HC/NO_x ratios (low NO_x levels). In the absence of seed, SOA mass increases with a shape of a sigmoidal curve.

The impact of RH on gasoline SOA formation was simulated using UNIPAR-CB6r3 for different seed conditions under the assumption of LLPS between the organic and the inorganic phases (Fig. 6(d)). In current, there is no process to predict aromatic SOA formation in salted solution in CMAQ-AE7. In the presence of wAS, a relatively large decrease in SOA yields appeared when the inorganic aerosol was effloresced at ERH (37% of ammonium sulfate (Tang and Munkelwitz, 1994)). Within our simulation ranges (RH > 30%), AHS has no phase transition. As reported in previous work (Zhou et al., 2019), SOA formation in the LLPS mode has little sensitivity to RH above ERH.

As seen in Fig. 6(e), aerosol acidity accelerates SOA growth via acid-catalyzed reactions of organic products (Jang et al., 2002). The efficiency of aerosol acidity on SOA growth differs in NO_x levels and HC ppb/seed mass. The impact of aerosol acidity is limited by the amount of reactive organic products. At our simulation condition, gasoline SOA growth shows a plateau (at 80% of maximum SOA mass) as seen in Fig. 6(e), and weak acidity is enough to lead to the maximum acidity effect. The effect of the quantity of wet seed (wAS and wAHS) on SOA formation is represented in Fig. 6(f). SOA mass drastically increases with increasing wAS when the wAS mass concentration is less than 20 µg m^{-3}. In a similar manner to aerosol acidity, SOA formation reaches to a plateau because heterogeneous reactions are limited to the quantity of reactive organic compounds. In the presence of AHS, SOA formation more quickly reaches to a plateau (5 µg m^{-3} of AHS) than that with wAS.

Figure 7 represents the uncertainties of the SOA prediction caused by the uncertainties in the major model parameters ($p_{L,i}^{\circ}$, $\gamma_{in,i}$, $k_{o,i}$, and $k_{AC,i}$) in the absence of GWP. At given conditions, $\gamma_{w,i}$ and $p_{L,i}^{\circ}$ are more significantly influential on SOA prediction than $k_{o,i}$, and $k_{AC,i}$. The uncertainty in $p_{L,i}^{\circ}$ was reported as 45% based on the group contributions. The gasoline SOA mass was influenced from -25 to 50 % by increasing/decreasing $p_{L,i}^{\circ}$ as a factor of 1.5/0.5. The uncertainty associated with $\gamma_{in,i}$ ranged from -28% to 18% by increasing/decreasing as a factor of 2/0.5. The estimated uncertainties of gasoline SOA from $k_{o,i}$ and $k_{AC,i}$ are relatively as small as -13 to 9 % by increasing/decreasing them as a factor of 1.5/0.5.

5 Atmospheric Implication

In this study, the gasoline SOA formation potential was simulated by using the UNIPAR-CB6r3 model under varying NO_x levels and seed conditions. UNIPAR-CB6r3 has a mechanism to predict SOA formation via CB6r3 gas mechanisms, gas–particle partitioning, and heterogeneous reaction in the absence of GWP bias. Through the model simulation, we conclude that both heterogeneous reactions in salted aqueous phase and the implementation of model parameters corrected for GWP are critical to accurately predict SOA mass. For example, SOA mass in Fig. 5 increases up to 1.8 times by using the

corrected model parameter on account of GWP bias. As seen in Fig. 6(e) and 6(f) (model sensitivity to seed conditions), SOA mass increases by three times from including 10 µg m^{-3} of wAS at 60% RH, in comparison to no-seeded SOA mass. The concentrations of SO$_2$ and sulfate have been rapidly declined due to innovative technologies and governmental efforts (Aas et al., 2019). However, the impact of the salted aqueous phase on SOA growth can be achieved even with a relatively small quantity of inorganic seed. For example, SOA formation from the photooxidation of 1500 ppbC of gasoline vapor can reach a plateau of 3-4 times higher organic mass with 5 µg m^{-3} of wAHS or 20 µg m^{-3} of wAS (Fig. 6(f)) under the high NO$_x$ level.

Electrolytic inorganic salts are ubiquitous in an urban atmosphere, because sulfate and nitrate are produced by the atmospheric oxidation of anthropogenic SO$_2$ and NO$_x$, respectively (Finlayson-Pitts and Pitts Jr, 1999). However, most current SOA modules are capable to simulate SOA formation via aqueous reactions only for a few reactive organic species (i.e., epoxydiol, glyoxal, and methylglyoxal). Numerous chemical species originating from the atmospheric oxidation of various precursors can be involved in aqueous reactions to form SOA. For example, the glyoxal fraction of the simulated gasoline SOA mass in Fig. 4(e) in the presence of wAS was about 40%, the methylglyoxal fraction was about 1%, and OM$_P$ was 26%. The remaining 23% associated with OM$_{AR}$ indicates a significant contribution of heterogeneous reactions of the reactive organic species other than glyoxal and methylglyoxal.

The liquid water content of PM$_{2.5}$ is high during regionally (i.e., eastern US) and seasonally (i.e., summer) humid conditions (Carlton et al., 2020). High humidity can shift the partitioning of hydrophilic organic gases toward the coexisting inorganic salted solution than to the organic phase, enhancing SOA growth via aqueous-reactions (Carlton and Turpin, 2013). When inorganic salt reaches the DRH (80% for AS (Brooks et al., 2002)), reactive organic species undergo aqueous phase reactions to form SOA. During warm periods at nighttime, inorganic salts can often be deliquesced in the eastern US and remain in aqueous solution above ERH. In arid areas where inorganic salts can be effloresced, SOA formation is depressed. Evidently, many field studies and model simulations have shown the greater amounts of SOA formation in eastern US in the summertime (Malm et al., 2017;Kelly et al., 2018), suggesting the important role of aqueous reactions on SOA formation.

In this study, the aerosol phase state is assumed to be LLPS for gasoline SOA formation in the presence of inorganic seed, because of hydrophobicity of some gasoline oxygenated products. The inorganic/organic mixed aerosol in the urban atmosphere, where automobile exhaust emissions and industrial solvents are abundant, may be governed in LLPS. Unlike SOA originating aromatics and terpenes, isoprene SOA is very polar and possibly mix with electrolytic aqueous solution to form a homogeneously mixed phase under the high humidity (Beardsley and Jang, 2016;Bertram et al., 2011). However, isoprene is not the only precursory HC to form SOA. For example, terpene, a biogenic HC, can coexist and form much less polar products than isoprene. The determination of the aerosol phase state is still controversial due to complex chemistry and precursors. LLPS likely appears in most urban areas and the regions that are influenced by high terpene emissions. In general, the atmospheric aging process increases the polarity and oligomeric matter in aerosol. Increased polarity increases organic solubility in the salted aqueous phase. However, oligomer is relatively unfavorable to be mixed with salted aqueous phase, in comparison to the low MW organics , because oligomers require a large combinational energy for mixing with small water molecules (Barton, 2017).

The organic products consumed to form SOA can influence gas mechanisms, although their quantity is little. Highly reactive organic species (i.e., glyoxal and multifunctional products in group VF and F) for heterogeneous chemistry to form SOA can also be quickly photolyzed in the gas phase. Thus, the consumed organics to form SOA can possibly influence concentrations of atmospheric oxidants and radicals. However, most SOA models including UNIPAR-CB6r3 are not capable of connecting carbon depletion to gas mechanisms due to SOA formation. This issue would potentially introduce inaccuracy in gas oxidation and aerosol prediction. Though the explicit approach (including detail gas oxidation mechanisms,

partitioning, and in-particle chemistry formation) is complex and time demanding, it improves a mass balance of organic products in multiphase reactions. In UNIPAR-CB6r3, the mathematical equations associated with stoichiometric coefficients of lumping species and their physicochemical parameters are inherited from explicit gas mechanisms. Thus, the model uncertainty can be caused by missing mechanisms in the gas phase. Additionally, the unidentified aerosol chemistry causes inaccuracy in SOA prediction and interpretation of aerosol formation mechanisms. For example, a recent study showed that the autoxidation of oxidized products can yield highly oxidized matter and increase SOA mass for certain precursors (i.e., terpenes) (Bianchi et al., 2019;Pye et al., 2019). Cross-reactions between RO_2 radicals can form accretion products (ROOR') with a low vapor pressure (Berndt et al., 2018).

Author contribution. MJ designed the experiments and MJ, SH carried them out. SH prepared the manuscript with contributions from MJ.

Competing interest. The authors declare that they have no conflict of interest.

Acknowledgments. This research was supported by awards from the National Science Foundation (NSF) (AGS1923651), National Institute of Environmental Research (NIER-2020-01-01-010), and the FRIEND (Fine Particle Research Initiative in East Asia Considering National Differences) Project through the National Research Foundation of Korea (NRF), funded by the Ministry of Science and ICT (2020M3G1A1114562).

References

Aas, W., Mortier, A., Bowersox, V., Cherian, R., Faluvegi, G., Fagerli, H., Hand, J., Klimont, Z., Galy-Lacaux, C., and Lehmann, C. M.: Global and regional trends of atmospheric sulfur, Scientific Reports, 9, 1-11, 2019.

Appel, K. W., Napelenok, S. L., Foley, K. M., Pye, H. O., Hogrefe, C., Luecken, D. J., Bash, J. O., Roselle, S. J., Pleim, J. E., and Foroutan, H.: Description and evaluation of the Community Multiscale Air Quality (CMAQ) modeling system version 5.1, Geoscientific Model Development, 10, 1703, 2017.

Appel, K. W., Bash, J. O., Fahey, K. M., Foley, K. M., Gilliam, R. C., Hogrefe, C., Hutzell, W. T., Kang, D., Mathur, R., and Murphy, B. N.: The Community Multiscale Air Quality (CMAQ) model versions 5.3 and 5.3. 1: system updates and evaluation, Geoscientific Model Development, 14, 2867-2897, 2021.

Baker, K., Carlton, A., Kleindienst, T., Offenberg, J., Beaver, M., Gentner, D., Goldstein, A., Hayes, P., Jimenez, J., and Gilman, J.: Gas and aerosol carbon in California: comparison of measurements and model predictions in Pasadena and Bakersfield, Atmospheric Chemistry and Physics, 15, 5243-5258, 2015.

Barton, A. F.: CRC handbook of solubility parameters and other cohesion parameters, Routledge, 2017.

Beardsley, R., and Jang, M.: Simulating the SOA formation of isoprene from partitioning and aerosol phase reactions in the presence of inorganics, Atmospheric Chemistry and Physics, 16, 5993-6009, 10.5194/acp-16-5993-2016, 2016.

Berndt, T., Scholz, W., Mentler, B., Fischer, L., Herrmann, H., Kulmala, M., and Hansel, A.: Accretion product formation from self-and cross-reactions of RO2 radicals in the atmosphere, Angewandte Chemie International Edition, 57, 3820-3824, 2018.

Bertram, A., Martin, S., Hanna, S., Smith, M., Bodsworth, A., Chen, Q., Kuwata, M., Liu, A., You, Y., and Zorn, S.: Predicting the relative humidities of liquid-liquid phase separation, efflorescence, and deliquescence of mixed particles of ammonium sulfate, organic material, and water using the organic-to-sulfate mass ratio of the particle and the oxygen-to-carbon elemental ratio of the organic component, Atmospheric Chemistry and Physics, 11, 2011.

Bianchi, F., Kurten, T., Riva, M., Mohr, C., Rissanen, M., Roldin, P., Berndt, T., Crounse, J., Wennberg, P., Mentel, T., Wildt, J., Junninen, H., Jokinen, T., Kulmala, M., Worsnop, D., Thornton, J., Donahue, N., Kjaergaard, H., and Ehn, M.: Highly Oxygenated Organic Molecules (HOM) from Gas-Phase Autoxidation Involving Peroxy Radicals: A Key Contributor to Atmospheric Aerosol, Chemical Reviews, 119, 3472-3509, 10.1021/acs.chemrev.8b00395, 2019.

Brooks, S. D., Wise, M. E., Cushing, M., and Tolbert, M. A.: Deliquescence behavior of organic/ammonium sulfate aerosol, Geophysical Research Letters, 29, 23-21-23-24, 2002.

Brune, W. H.: The Chamber Wall Index for Gas–Wall Interactions in Atmospheric Environmental Enclosures, Environmental Science & Technology, 53, 3645-3652, 2019.

Cao, G., and Jang, M.: An SOA model for toluene oxidation in the presence of inorganic aerosols, Environmental Science & Technology, 44, 727-733, 2010.

Cappa, C. D., Jathar, S. H., Kleeman, M. J., Docherty, K. S., Jimenez, J. L., Seinfeld, J. H., and Wexler, A. S.: Simulating secondary organic aerosol in a regional air quality model using the statistical oxidation model–Part 2: Assessing the influence of vapor wall losses, Atmospheric Chemistry and Physics, 16, 2016.

Carlton, A., and Turpin, B.: Particle partitioning potential of organic compounds is highest in the Eastern US and driven by anthropogenic water, Atmospheric Chemistry and Physics, 13, 10203-10214, 2013.

Carlton, A. G., Bhave, P. V., Napelenok, S. L., Edney, E. O., Sarwar, G., Pinder, R. W., Pouliot, G. A., and Houyoux, M.: Model representation of secondary organic aerosol in CMAQv4. 7, Environmental Science & Technology, 44, 8553-8560, 2010.

Carlton, A. G., Christiansen, A. E., Flesch, M. M., Hennigan, C. J., and Sareen, N.: Mulitphase Atmospheric Chemistry in Liquid Water: Impacts and Controllability of Organic Aerosol, Accounts of Chemical Research, 53, 1715-1723, 2020.

450 Cohen, A., Brauer, M., Burnett, R., Anderson, H., Frostad, J., Estep, K., Balakrishnan, K., Brunekreef, B., Dandona, L., Dandona, R., Feigin, V., Freedman, G., Hubbell, B., Jobling, A., Kan, H., Knibbs, L., Liu, Y., Martin, R., Morawska, L., Pope, C., Shin, H., Straif, K., Shaddick, G., Thomas, M., van Dingenen, R., van Donkelaar, A., Vos, T., Murray, C., and Forouzanfar, M.: Estimates and 25-year trends of the global burden of disease attributable to ambient air pollution: an analysis of data from the Global Burden of Diseases Study 2015, Lancet, 389, 1907-1918, 10.1016/S0140-6736(17)30505-

455 6, 2017.

Cox, R. A., and Yates, K.: Kinetic equations for reactions in concentrated aqueous acids based on the concept of" excess acidity", Canadian Journal of Chemistry, 57, 2944-2951, 1979.

Damian, V., Sandu, A., Damian, M., Potra, F., and Carmichael, G. R.: The kinetic preprocessor KPP-a software environment for solving chemical kinetics, Computers & Chemical Engineering, 26, 1567-1579, 2002.

460 De Schrijver, F., and Smets, G.: Polymerization kinetics in highly viscous media, Journal of Polymer Science Part A-1: Polymer Chemistry, 4, 2201-2210, 1966.

Donahue, N., Robinson, A., Stanier, C., and Pandis, S.: Coupled partitioning, dilution, and chemical aging of semivolatile organics, Environmental Science & Technology, 40, 2635-2643, 10.1021/es052297c, 2006.

Dzepina, K., Cappa, C. D., Volkamer, R. M., Madronich, S., DeCarlo, P. F., Zaveri, R. A., and Jimenez, J. L.: Modeling the

465 multiday evolution and aging of secondary organic aerosol during MILAGRO 2006, Environmental Science & Technology, 45, 3496-3503, 2011.

Emmerson, K., and Evans, M.: Comparison of tropospheric gas-phase chemistry schemes for use within global models, Atmospheric Chemistry and Physics, 9, 2009.

Ensberg, J., Hayes, P., Jimenez, J., Gilman, J., Kuster, W., De Gouw, J., Holloway, J., Gordon, T., Jathar, S., and Robinson,

470 A.: Emission factor ratios, SOA mass yields, and the impact of vehicular emissions on SOA formation, Atmospheric Chemistry and Physics, 14, 2383-2387, 2014.

Finlayson-Pitts, B. J., and Pitts Jr, J. N.: Chemistry of the upper and lower atmosphere: theory, experiments, and applications, Elsevier, 1999.

Gentner, D. R., Jathar, S. H., Gordon, T. D., Bahreini, R., Day, D. A., El Haddad, I., Hayes, P. L., Pieber, S. M., Platt, S. M.,

475 and de Gouw, J.: Review of urban secondary organic aerosol formation from gasoline and diesel motor vehicle emissions, Environmental Science & Technology, 51, 1074-1093, 2017.

Gross, D. S., Gälli, M. E., Kalberer, M., Prevot, A. S., Dommen, J., Alfarra, M. R., Duplissy, J., Gaeggeler, K., Gascho, A., and Metzger, A.: Real-time measurement of oligomeric species in secondary organic aerosol with the aerosol time-of-flight mass spectrometer, Analytical Chemistry, 78, 2130-2137, 2006.

480 Hall IV, W. A., and Johnston, M. V.: Oligomer content of α-pinene secondary organic aerosol, Aerosol Science and Technology, 45, 37-45, 2011.

Hallquist, M., Wenger, J., Baltensperger, U., Rudich, Y., Simpson, D., Claeys, M., Dommen, J., Donahue, N., George, C., Goldstein, A., Hamilton, J., Herrmann, H., Hoffmann, T., Iinuma, Y., Jang, M., Jenkin, M., Jimenez, J., Kiendler-Scharr, A., Maenhaut, W., McFiggans, G., Mentel, T., Monod, A., Prevot, A., Seinfeld, J., Surratt, J., Szmigielski, R., and Wildt, J.:

485 The formation, properties and impact of secondary organic aerosol: current and emerging issues, Atmospheric Chemistry and Physics, 9, 5155-5236, 10.5194/acp-9-5155-2009, 2009.

Han, S., and Jang, M.: Simulating the impact of gas-wall partitioning on SOA formation using the explicit gas mechanism integrated with aqueous reactions containing electrolytes, Science of The Total Environment, 748, 141360, 2020.

Hayes, P. L., Carlton, A. G., Baker, K. R., Ahmadov, R., Washenfelder, R. A., Alvarez, S., Rappenglück, B., Gilman, J. B.,

490 Kuster, W., and De Gouw, J. A.: Modeling the formation and aging of secondary organic aerosols in Los Angeles during CalNex 2010, Atmospheric Chemistry and Physics, 15, 5773-5801, 2015.

Heald, C., Henze, D., Horowitz, L., Feddema, J., Lamarque, J. F., Guenther, A., Hess, P., Vitt, F., Seinfeld, J., and Goldstein,

A.: Predicted change in global secondary organic aerosol concentrations in response to future climate, emissions, and land use change, Journal of Geophysical Research: Atmospheres, 113, 2008.

495   Huang, Y., Zhao, R., Charan, S., Kenseth, C., Zhang, X., and Seinfeld, J.: Unified Theory of Vapor-Wall Mass Transport in Teflon-Walled Environmental Chambers, Environmental Science & Technology, 52, 2134-2142, 10.1021/acs.est.7b05575, 2018.

Im, Y., Jang, M., and Beardsley, R.: Simulation of aromatic SOA formation using the lumping model integrated with explicit gas-phase kinetic mechanisms and aerosol-phase reactions, Atmospheric Chemistry and Physics, 14, 2014.

500   Jang, M., Czoschke, N., Lee, S., and Kamens, R.: Heterogeneous atmospheric aerosol production by acid-catalyzed particle-phase reactions, Science, 298, 814-817, 10.1126/science.1075798, 2002.

Jang, M., Czoschke, N. M., and Northcross, A. L.: Semiempirical model for organic aerosol growth by acid-catalyzed heterogeneous reactions of organic carbonyls, Environmental Science & Technology, 39, 164-174, 2005.

Jang, M., Czoschke, N. M., Northcross, A. L., Cao, G., and Shaof, D.: SOA formation from partitioning and heterogeneous
505   reactions: model study in the presence of inorganic species, Environmental science & technology, 40, 3013-3022, 2006.

Jang, M., Sun, S., Winslow, R., Han, S., and Yu, Z.: In situ aerosol acidity measurements using a UV–Visible micro-spectrometer and its application to the ambient air, Aerosol Science and Technology, 54, 446-461, 2020.

Jathar, S. H., Mahmud, A., Barsanti, K. C., Asher, W. E., Pankow, J. F., and Kleeman, M. J.: Water uptake by organic aerosol and its influence on gas/particle partitioning of secondary organic aerosol in the United States, Atmospheric
510   Environment, 129, 142-154, 2016.

Jenkin, M., Wyche, K., Evans, C., Carr, T., Monks, P., Alfarra, M., Barley, M., McFiggans, G., Young, J., and Rickard, A.: Development and chamber evaluation of the MCM v3.2 degradation scheme for beta-caryophyllene, Atmospheric Chemistry and Physics, 12, 5275-5308, 10.5194/acp-12-5275-2012, 2012.

Jerrett, M., Burnett, R. T., Pope III, C. A., Ito, K., Thurston, G., Krewski, D., Shi, Y., Calle, E., and Thun, M.: Long-term
515   ozone exposure and mortality, New England Journal of Medicine, 360, 1085-1095, 2009.

Jimenez, J. L., Canagaratna, M., Donahue, N., Prevot, A., Zhang, Q., Kroll, J. H., DeCarlo, P. F., Allan, J. D., Coe, H., and Ng, N.: Evolution of organic aerosols in the atmosphere, Science, 326, 1525-1529, 2009.

Kalberer, M., Paulsen, D., Sax, M., Steinbacher, M., Dommen, J., Prévôt, A. S., Fisseha, R., Weingartner, E., Frankevich, V., and Zenobi, R.: Identification of polymers as major components of atmospheric organic aerosols, Science, 303, 1659-1662,
520   2004.

Kalberer, M., Sax, M., and Samburova, V.: Molecular size evolution of oligomers in organic aerosols collected in urban atmospheres and generated in a smog chamber, Environmental Science & Technology, 40, 5917-5922, 2006.

Kelly, J. M., Doherty, R. M., O'Connor, F. M., and Mann, G. W.: The impact of biogenic, anthropogenic, and biomass burning volatile organic compound emissions on regional and seasonal variations in secondary organic aerosol,
525   Atmospheric Chemistry and Physics, 18, 7393-7422, 2018.

Koop, T., Bookhold, J., Shiraiwa, M., and Pöschl, U.: Glass transition and phase state of organic compounds: dependency on molecular properties and implications for secondary organic aerosols in the atmosphere, Physical Chemistry Chemical Physics, 13, 19238-19255, 2011.

Krechmer, J., Pagonis, D., Ziemann, P., and Jimenez, J.: Quantification of Gas-Wall Partitioning in Teflon Environmental
530   Chambers Using Rapid Bursts of Low-Volatility Oxidized Species Generated in Situ, Environmental Science & Technology, 50, 5757-5765, 10.1021/acs.est.6b00606, 2016.

Krechmer, J. E., Day, D. A., and Jimenez, J. L.: Always Lost but Never Forgotten: Gas-Phase Wall Losses Are Important in All Teflon Environmental Chambers, Environmental Science & Technology, 54, 12890-12897, 2020.

Li, J., and Jang, M.: Aerosol acidity measurement using colorimetry coupled with a reflectance UV-visible spectrometer,
535   Aerosol Science and Technology, 46, 833-842, 2012.

Li, W., Li, L., Chen, C.-l., Kacarab, M., Peng, W., Price, D., Xu, J., and Cocker III, D. R.: Potential of select intermediate-volatility organic compounds and consumer products for secondary organic aerosol and ozone formation under relevant urban conditions, Atmospheric Environment, 178, 109-117, 2018.

Malm, W. C., Schichtel, B. A., Hand, J. L., and Collett Jr, J. L.: Concurrent temporal and spatial trends in sulfate and organic mass concentrations measured in the IMPROVE monitoring program, Journal of Geophysical Research: Atmospheres, 122, 10,462-410,476, 2017.

Matsunaga, A., and Ziemann, P.: Gas-Wall Partitioning of Organic Compounds in a Teflon Film Chamber and Potential Effects on Reaction Product and Aerosol Yield Measurements, Aerosol Science and Technology, 44, 881-892, 10.1080/02786826.2010.501044, 2010.

McDonald, B. C., de Gouw, J. A., Gilman, J. B., Jathar, S. H., Akherati, A., Cappa, C. D., Jimenez, J. L., Lee-Taylor, J., Hayes, P. L., and McKeen, S. A.: Volatile chemical products emerging as largest petrochemical source of urban organic emissions, Science, 359, 760-764, 2018.

Odian, G.: Principles of polymerization, John Wiley & Sons, 2004.

Odum, J., Hoffmann, T., Bowman, F., Collins, D., Flagan, R., and Seinfeld, J.: Gas/particle partitioning and secondary organic aerosol yields, Environmental Science & Technology, 30, 2580-2585, 10.1021/es950943+, 1996.

Pankow, J. F.: An absorption model of the gas/aerosol partitioning involved in the formation of secondary organic aerosol, Atmospheric Environment, 28, 189-193, 1994.

Pöschl, U.: Atmospheric aerosols: composition, transformation, climate and health effects, Angewandte Chemie International Edition, 44, 7520-7540, 2005.

Press, W. H., Teukolsky, S. A., Flannery, B. P., and Vetterling, W. T.: Numerical recipes in Fortran 77: volume 1, volume 1 of Fortran numerical recipes: the art of scientific computing, Cambridge university press, 1992.

Pye, H. O., Murphy, B. N., Xu, L., Ng, N. L., Carlton, A. G., Guo, H., Weber, R., Vasilakos, P., Appel, K. W., and Budisulistiorini, S. H.: On the implications of aerosol liquid water and phase separation for organic aerosol mass, Atmospheric Chemistry and Physics, 17, 343-369, 2017.

Pye, H. O., D'Ambro, E. L., Lee, B. H., Schobesberger, S., Takeuchi, M., Zhao, Y., Lopez-Hilfiker, F., Liu, J., Shilling, J. E., and Xing, J.: Anthropogenic enhancements to production of highly oxygenated molecules from autoxidation, Proceedings of the National Academy of Sciences, 116, 6641-6646, 2019.

Qin, M., Murphy, B. N., Isaacs, K. K., McDonald, B. C., Lu, Q., McKeen, S. A., Koval, L., Robinson, A. L., Efstathiou, C., and Allen, C.: Criteria pollutant impacts of volatile chemical products informed by near-field modelling, Nature Sustainability, 4, 129-137, 2021.

Reid, J. P., Bertram, A. K., Topping, D. O., Laskin, A., Martin, S. T., Petters, M. D., Pope, F. D., and Rovelli, G.: The viscosity of atmospherically relevant organic particles, Nature Communications, 9, 1-14, 2018.

Schell, B., Ackermann, I. J., Hass, H., Binkowski, F. S., and Ebel, A.: Modeling the formation of secondary organic aerosol within a comprehensive air quality model system, Journal of Geophysical Research: Atmospheres, 106, 28275-28293, 2001.

Shah, R. U., Coggon, M. M., Gkatzelis, G. I., McDonald, B. C., Tasoglou, A., Huber, H., Gilman, J., Warneke, C., Robinson, A. L., and Presto, A. A.: Urban oxidation flow reactor measurements reveal significant secondary organic aerosol contributions from volatile emissions of emerging importance, Environmental Science & Technology, 54, 714-725, 2019.

Shiraiwa, M., Ammann, M., Koop, T., and Pöschl, U.: Gas uptake and chemical aging of semisolid organic aerosol particles, Proceedings of the National Academy of Sciences, 108, 11003-11008, 2011.

Shiraiwa, M., and Seinfeld, J. H.: Equilibration timescale of atmospheric secondary organic aerosol partitioning, Geophysical Research Letters, 39, 2012.

Stein, S., and Brown, R.: Estimation of normal boiling points from group contributions, Journal of Chemical Information

and Computer Sciences, 34, 581-587, 10.1021/ci00019a016, 1994.

580 Tang, I., and Munkelwitz, H.: Aerosol phase transformation and growth in the atmosphere, Journal of Applied Meteorology, 33, 791-796, 1994.

Tolocka, M., Jang, M., Ginter, J., Cox, F., Kamens, R., and Johnston, M.: Formation of oligomers in secondary organic aerosol, Environmental Science & Technology, 38, 1428-1434, 10.1021/es035030r, 2004.

Turner, M. C., Jerrett, M., Pope III, C. A., Krewski, D., Gapstur, S. M., Diver, W. R., Beckerman, B. S., Marshall, J. D., Su,

585 J., and Crouse, D. L.: Long-term ozone exposure and mortality in a large prospective study, American journal of respiratory and critical care medicine, 193, 1134-1142, 2016.

Volkamer, R., Jimenez, J., San Martini, F., Dzepina, K., Zhang, Q., Salcedo, D., Molina, L., Worsnop, D., and Molina, M.: Secondary organic aerosol formation from anthropogenic air pollution: Rapid and higher than expected, Geophysical Research Letters, 33, 10.1029/2006GL026899, 2006.

590 Woody, M. C., Baker, K. R., Hayes, P. L., Jimenez, J. L., Koo, B., and Pye, H. O.: Understanding sources of organic aerosol during CalNex-2010 using the CMAQ-VBS, Atmospheric Chemistry and Physics, 16, 4081-4100, 2016.

Yarwood, G., Rao, S., Yocke, M., and Whitten, G.: Updates to the carbon bond mechanism: CB05, Report to the US Environmental Protection Agency. RT-04, 675, 2005.

Yarwood, G., Jung, J., Whitten, G. Z., Heo, G., Mellberg, J., and Estes, M.: Updates to the Carbon Bond mechanism for

595 version 6 (CB6), 9th Annual CMAS Conference, Chapel Hill, NC, 2010, 11-13,

Yeh, G., and Ziemann, P.: Gas-Wall Partitioning of Oxygenated Organic Compounds: Measurements, Structure-Activity Relationships, and Correlation with Gas Chromatographic Retention Factor, Aerosol Science and Technology, 49, 726-737, 10.1080/02786826.2015.1068427, 2015.

Yu, Z., Jang, M., Zhang, T., Madhu, A., and Han, S.: Simulation of Monoterpene SOA Formation by Multiphase Reactions

600 Using Explicit Mechanisms, ACS Earth and Space Chemistry, 2021.

Zhang, X., Cappa, C., Jathar, S., Mcvay, R., Ensberg, J., Kleeman, M., and Seinfeld, J.: Influence of vapor wall loss in laboratory chambers on yields of secondary organic aerosol, Proceedings of the National Academy of Sciences of the United States of America, 111, 5802-5807, 10.1073/pnas.1404727111, 2014.

Zhou, C., Jang, M., and Yu, Z.: Simulation of SOA formation from the photooxidation of monoalkylbenzenes in the

605 presence of aqueous aerosols containing electrolytes under various NO x levels, Atmospheric Chemistry and Physics, 19, 5719-5735, 2019.

Zuend, A., Marcolli, C., Booth, A., Lienhard, D. M., Soonsin, V., Krieger, U., Topping, D. O., McFiggans, G., Peter, T., and Seinfeld, J. H.: New and extended parameterization of the thermodynamic model AIOMFAC: calculation of activity coefficients for organic-inorganic mixtures containing carboxyl, hydroxyl, carbonyl, ether, ester, alkenyl, alkyl, and

610 aromatic functional groups, Atmospheric Chemistry and Physics, 11, 9155-9206, 2011.

Table 1. Experimental conditions for the photooxidation of the gasoline in the UF-APHOR chamber.

Date (Chamber ID)	Initial condition					Temp (K)	%RH	max OM ($\mu g\ m^{-3}$)	Max TUVR (W m^{-2})[e]	Figure
	HC[a] (ppbC)	HC/NO$_x$ (ppbC/ppb)	Seed[b]	Seed mass[c] ($\mu g\ m^{-3}$)	OM$_0$[d] ($\mu g\ m^{-3}$)					
12/5/2020 (E)	1800	12.8	NS	-	2	281-302	46-98	13.4	19.9	4(a), 5(a)
3/6/2019 (W)	1500	11.0	SA	30	2	290-315	28-91	9.6	31.9	4(d)
1/16/2021 (E)	1500	12.5	dAS	50	2	275-296	24-86	7.9	21.3	4(e)
1/16/2021 (W)	1500	12.5	wAS	50	2	276-296	60-93	20.07	21.3	4(e), 5(d)
1/19/2021 (E)	1500	12.2	wAS	120	3	274-300	47-88	22.8	20.4	4(f)
1/4/2021 (E)	1500	2	SA	30	4	277-300	26-88	8.9	21.1	4(b), 5(b)
1/4/2021 (W)	1500	2.3	NS	-	4	278-301	32-93	6.6	21.1	4(c), 5(c)
1/28/2021 (E)	1500	6.8	wAS	30	1.5	279-297	31-91	10.1	23.6	4(g)

[a] Total HC concentrations in gasoline injected into the chamber. The HC concentrations were determined by using GC/FID (Fig. S1).

615   [b] NS, SA, wAS, and dAS indicate non-seeded, sulfuric acid seed, wet ammonium sulfate seed, and dry ammonium sulfate seed, respectively.

[c] The seed mass is determined as a dry mass, without water mass.

[d] The pre-existing organic matter (OM$_0$) is determined for the chamber air prior to the injection of inorganic seed and HC.

[e] Total ultra violet radiation (TUVR) measured solar ultra violet radiation (W m^{-2}). The measured solar ultra violet radiation

620   on 12/5/2020 and 3/6/2019 are shown in the Fig. S5 (b).
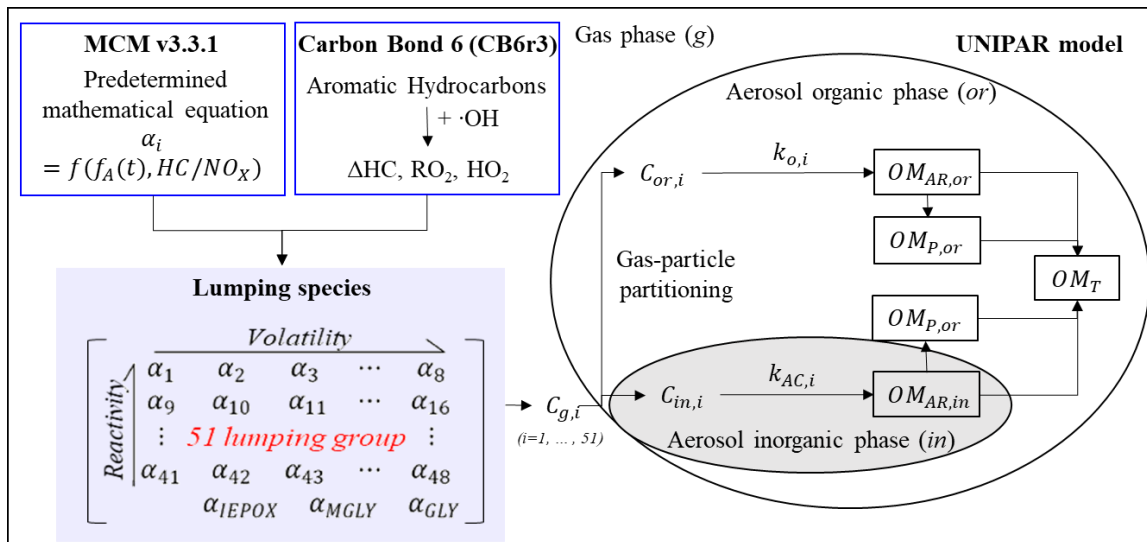
Figure 1. The structure of the UNIPAR-CB6r3 to predict the gasoline SOA formation. $C_{g,i}$, $C_{or,i}$, and $C_{in,i}$ are the concentration of organic compound (i) in gas phase (g), organic phase (or), and inorganic phase (in). The dynamic stoichiometric coefficient (dynamic α_i), the consumption of HC (ΔHC), the concentration of hydroperoxide radical ([HO$_2$]), and the concentration of organic peroxyl radical ([RO$_2$]) are simulated from the CB6r3. The aging scale factor (f_A) is represented as a function of [HO$_2$], [RO$_2$], and the initial concentration of HC (Zhou et al., 2019). OM$_{AR}$, OM$_P$, and OM$_T$ indicate organic matters (OM) formed from aerosol-phase reactions, OM formed from the partitioning process, and total OM, respectively.
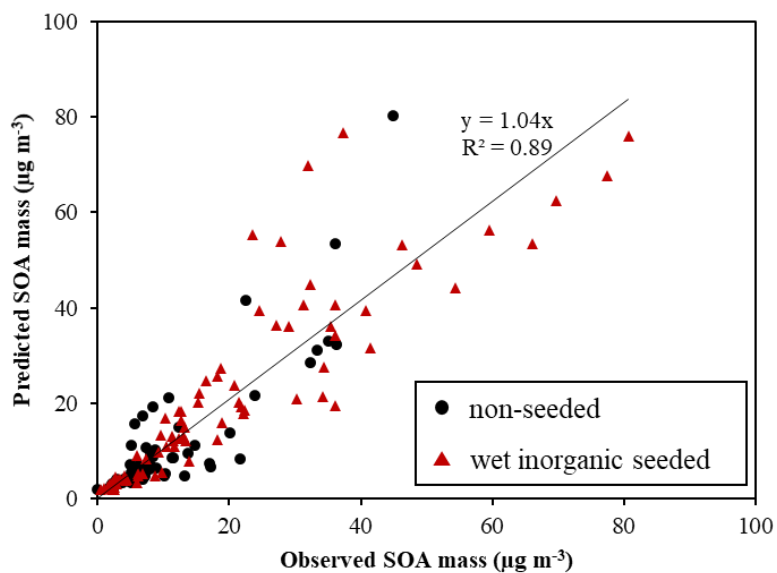
Figure 2. The linearity of predicted SOA mass (µg m^{-3}) using UNIPAR-CB6r3 and observed SOA mass (µg m^{-3}) in the
635 absence and the presence of wet inorganic seed. SOA mass was produced via the photooxidation of various aromatic HCs
(Table S2) in the UF-APHOR chamber.
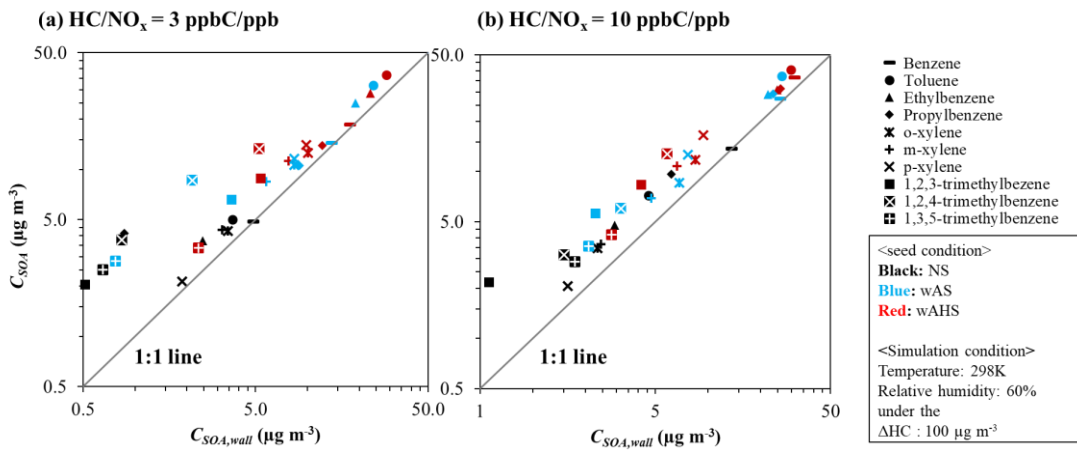
Figure 3. The simulated C_{SOA} and $C_{SOA,wall}$ for 10 different aromatic HCs at the given reference conditions. The SOA formation is simulated at the 298K and 60% at a given sunlight intensity (Fig. S5(a)). The concentration of initial HC is determined to consume 100 µg m^{-3} of HC at 5PM. The initial HC ppbC/NO$_x$ ppb sets to 3 and 10 for high NO$_x$ level and low NO$_x$ level, respectively. SOA masses are also obtained at 5PM. The color of the symbol indicates the seed conditions: black, blue, and red for non-seeded (NS), wet ammonium sulfate (wAS), and wet ammonium hydrogen sulfate (wAHS), respectively.
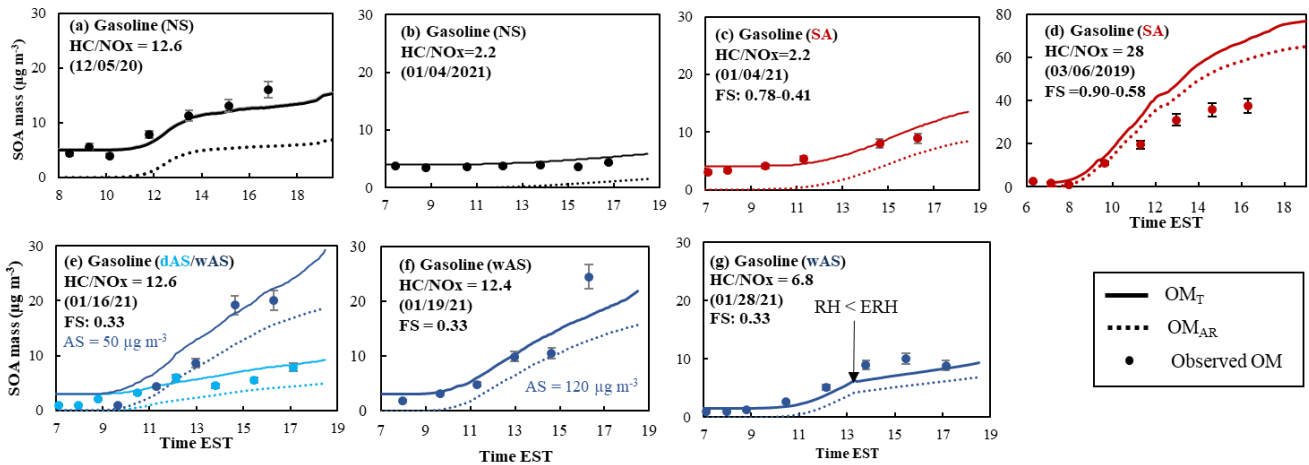
Figure 4. Observed (symbol) and simulated SOA mass using UNIPAR-CB6r3 (line) for the photooxidation of gasoline vapor at different NO_x levels. SOA mass concentrations are corrected for the particle loss to the chamber wall. The simulated OM_T (solid line) and OM_{AR} (dotted line) are also illustrated. The error (9%) associated with SOA mass was estimated with the instrumental uncertainty in the OC/EC analyzer. SOA mass was produced via the photooxidation of gasoline vapor (Table 1) in the UF-APHOR chamber. The averaged deviations of simulation from experimental data are (a) 2%, (b) -14%, (c) -32%, (d) -22% and -24%, (e) -10%, and (f) 10%.
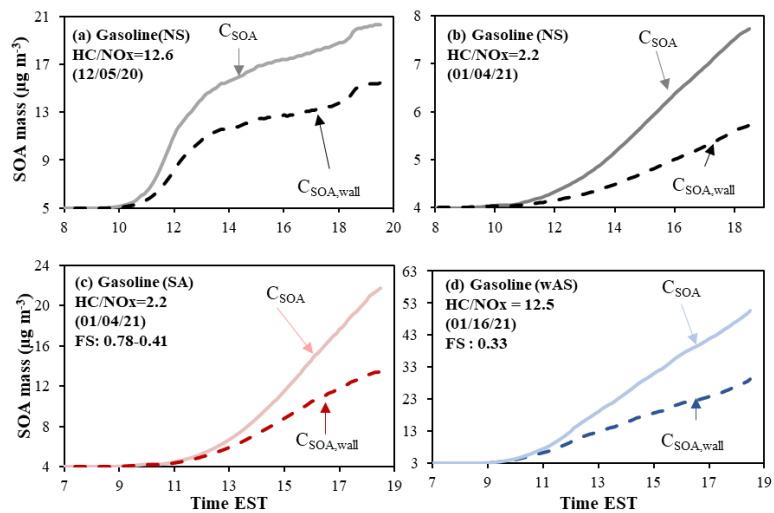
Figure 5. The comparison of gasoline SOA mass ($C_{SOA,wall}$) in the presence of GWP and gasoline SOA mass (C_{SOA}) in the absence of GWP. SOA formation was simulated using UNIPAR-CB6r3 for the photooxidation of gasoline vapor at given experimental conditions (Table 1).
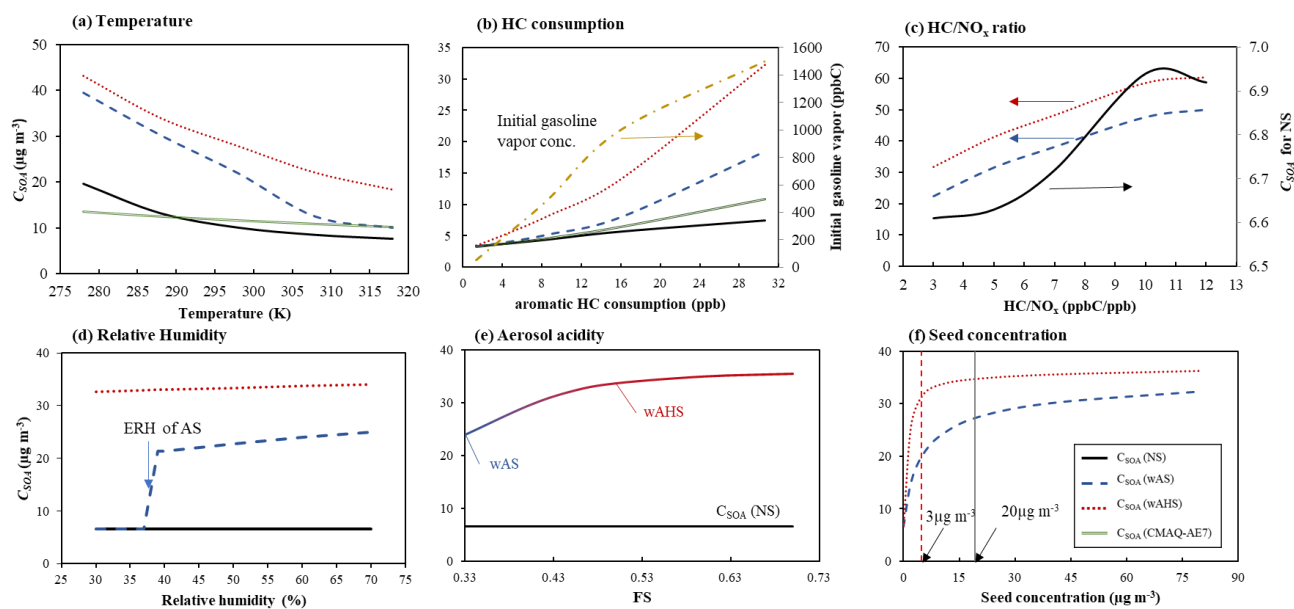
Figure 6. Sensitivities of simulated gasoline SOA mass to (a) temperature, (b) aromatic HC consumption, (c) HC/ NO_x ratio, (d) relative humidity, (e) aerosol acidity, and (f) seed concentrations. SOA mass is simulated at the high NO_x level (HC/NO_x= 3 ppbC/ppb) under given reference conditions (298K, 60% RH, and 1500 ppbC of gasoline vapor) under the specific sunlight intensity measured on 06/19/2015 (Fig. S5(a)). The concentrations of OM_0 and inorganic seed are 3 µg m^{-3} and 10 µg m^{-3}, respectively. The simulated SOA mass using UNIPAR-CB6r3 was compared to that using CMAQ-AE7 module in (a) and (b).
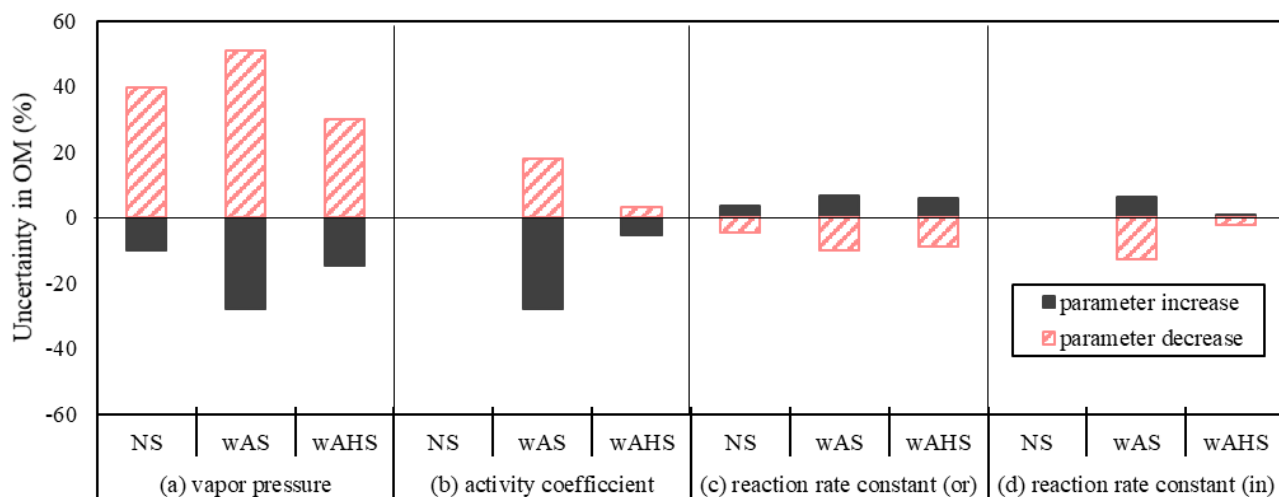
Figure 7. Uncertainties in UNIPAR-CB6r3 simulated gasoline SOA mass due to model parameters: (a) vapor pressure ($P_{L,i}$), (b) activity coefficient in inorganic phase (γ_{in}), (c) aerosol phase reaction rate constant in organic phase (k_o), and (d) aqueous phase reaction rate constant (k_{AC}). The errors associated with $P_{L,i}$, k_{AC}, and k_o were estimated by increasing and decreasing the factors by 150 and 50%. The uncertainties associated with γ_{in} were estimated through increasing and decreasing γ_{in} by 200 and 50%, respectively. The SOA formation was simulated at the high NO$_x$ level (HC/NO$_x$= 3 ppbC/ppb) under the given reference conditions (298K, 60% RH, and 1500 ppbC of gasoline vapor) under the specific sunlight intensity measured on 06/19/2015 (Fig. S5(a)). The concentration of pre-existing organic matter and inorganic seed was 3 µg m^{-3} and 10 µg m^{-3}, respectively.